Chemosphere 226 (2019) 159–165

Contents lists available at ScienceDirect

Chemosphere

journal homepage: www.elsevier.com/locate/chemosphere

The critical factors affecting typical organophosphate flame retardants to mimetic biomembrane: An integrated *in vitro* and *in silico* study

Xiaoqing Wang [a, c], Xiangjing Meng [a, c], Fei Li [a, *], Jiawang Ding [a], Chenglong Ji [a], Huifeng Wu [a, b]

[a] CAS Key Laboratory of Coastal Environmental Processes and Ecological Remediation, Yantai Institute of Coastal Zone Research (YIC), Chinese Academy of Sciences(CAS), Shandong Key Laboratory of Coastal Environmental Processes, YICCAS, Yantai, 264003, PR China
[b] Laboratory for Marine Fisheries Science and Food Production Processes, Qingdao National Laboratory for Marine Science and Technology, Qingdao, 266237, PR China
[c] University of Chinese Academy of Sciences, Beijing, 100049, PR China

HIGHLIGHTS

- OPFRs induced cytotoxicity in a structure-dependent manner.
- The key factors affecting OPFRs to mimetic biomembrane were screened by QSAR model.
- QSAR model had good robustness and mechanism interpretability.
- OPFRs with strong electronegativity could destroy membrane's integrity.
- Steric effect could impair the damage capacity caused by electronegativity.

GRAPHICAL ABSTRACT

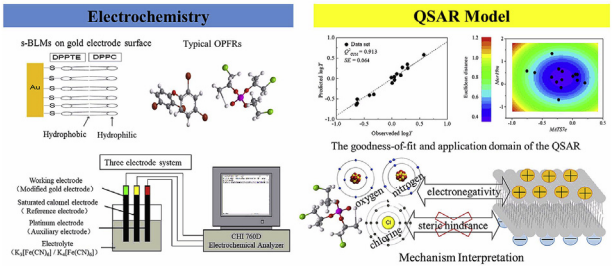

ARTICLE INFO

Article history:
Received 29 January 2019
Received in revised form
18 March 2019
Accepted 19 March 2019
Available online 23 March 2019

Handling Editor: Prof Willie Peijnenburg

Keywords:
Organophosphate flame retardants (OPFRs)
Quantitative structure-activity relationship (QSAR)
Mimetic biomembrane
Electrochemical impedance spectroscopy (EIS)
Partial least squares (PLS)

ABSTRACT

Organophosphate flame retardants (OPFRs) have been reported to induce cytotoxicity in a structure-dependent manner. The toxic effects may be due to the damage of biomembrane integrity and/or the interference of membrane signal pathway. In this study, the damages of fifteen typical OPFRs (chlorinated phosphates, alkyl phosphates, aryl phosphates, and alkoxy phosphates) to mimetic biomembrane were determined by the electrochemical impedance spectroscopy (EIS). The molecular structure descriptors that characterized the action mechanisms were screened by stepwise regression. The six molecular descriptors (*MATS7e*, *DLS_05*, *Mor19m*, *Mor22v*, *Mor12v* and *MATS8m*) were screened to study the actions between OPFRs and mimetic biomembrane. A quantitative structure-activity relationship (QSAR) model was developed by the partial least squares (PLS) method. Statistical results indicated that the QSAR model had good robustness and mechanism interpretability. The distribution of atomic electronegativities (*MATS7e*) and atomic masses in three dimensional spaces (*Mor19m*) were the key factors influencing the actions between OPFRs and simulated biofilms. The compounds with strong electron-withdrawing property could invade the inner layer of membrane and destroy its integrity. High levels of steric hindrance could impair the damage capacity caused by electronegativity. Moreover, drug-like index (*DLS_05*), spatial structures of particle (*Mor22v*, *Mor12v*) and atomic masses (*MATS8m*) also affected the actions. The results revealed the mechanism of the actions of OPFRs with simulated biofilms and elucidated the key structural characteristics affecting the actions of OPFRs, which could provide theoretical basis for ecological risk assessment of OPFRs.

* Corresponding author.
E-mail address: fli@yic.ac.cn (F. Li).

https://doi.org/10.1016/j.chemosphere.2019.03.130
0045-6535/

1. Introduction

Organophosphate flame retardants (OPFRs) are being increasingly consumed with its excellent flame retardant and plasticizing properties (Moller et al., 2012; van der Veen and de Boer, 2012). According to the European Flame Retardants Association (EFRA) statistics, the sales of OPFRs were far exceeded BFRs between the years of 2004 and 2006 in Europe and OPFRs had become an emerging contaminants (Kim et al., 2013). OPFRs are not covalently bound in the host polymer materials and can more easily leach into the environmental matrices via volatilization, leaching or abrasion (Marklund et al., 2003; Van den Eede et al., 2011). Depending on different substitutes, OPFRs are divided into alkyl phosphates, aryl phosphates, chlorinated phosphates, and halogenated phosphates. Different substituted OPFRs have diverse physical and chemical characteristics and application fields. Chlorinated OPFRs with higher polarities and higher vapor pressures, such as tris(2-chloroethyl) phosphate (TCEP) and tris(1-chloro-2-propyl) phosphate (TCPP), are mainly used as flame retardants in the fireproofed material (Reemtsma et al., 2008; van der Veen and de Boer, 2012). Aryl and alkyl-OPFRs with higher molecular mass such as triphenyl phosphate (TPP) and 2-ethylhexyl diphenyl phosphate (EHDPP) are more hydrophobic (Van den Eede et al., 2011; van der Veen and de Boer, 2012), which make OPFRs prevalently exist in the environment.

Toxicological studies had shown that OPFRs could induce neurotoxicity (Dishaw et al., 2011), cytotoxicity (Chen et al., 2015; Ren et al., 2008), endocrine disrupting effects (Zhang et al., 2014), and carcinogenic effects (van der Veen and de Boer, 2012). Toxicity of OPFRs were closely related to substituent groups. Compared with alkyl group substituted OPFRs, the OPFRs substituted with aromatic or chlorinated alkyl groups could inhibit O-linked N-acetylglucosamine (O-GlcNAc) transferase (OGT) (Gu et al., 2018) and lysine decarboxylase (LDC) (Wang et al., 2014) activity significantly. The biotransformation of OPFRs substituted with chlorinated alkyl or aromatic chains could more significantly affect the accumulation than those with alkyl chains based on the physiologically based toxicokinetic (PBTK) model (Wang et al., 2017a). The phenyl rings of TPP inserted into active pockets with tightly binding affinity which showed significant estrogenic activities to human estrogen receptor α (*h*ERα) (Zhang et al., 2014).

As the barrier against the environment, the biomembrane is an important place for matter exchange and information transfer. Previous studies showed that pollutants could directly damage the integrity of biomembrane and/or interrupt the membrane signal pathway to exert toxic hazard. Exposed to high concentrations of tributyl phosphate (TBP) and tris(2-butoxyethyl) phosphate (TBEP), the abnormalities and destruction of biomembrane of human liver cancer cells (HepG2) were observed (Ren et al., 2017). DnBP could interfere with thyroid hormone homeostasis via membrane receptor (integrin $\alpha v\beta 3$) and ERK 1/2 signal pathway to induce cell proliferation (Kong et al., 2018). Understanding on the different substituent groups affecting the actions between OPFRs and biofilms is essential to thoroughly evaluate the toxicity mechanism of OPFRs.

It was reported that the mimetic biofilms such as the supported bilayer lipid membrane (s-BLM) had good electrochemical properties and stability to illuminate the actions between the membrane and the compounds (Wu and Jiang, 2016). As one of electrochemical techniques, electrochemical impedance spectroscopy (EIS) could effectively characterize the structural changes of s-BLM (Chen et al., 2012; Harris and Bruening, 2000). This method has been used to study the interaction between curcumin and simulated biofilm (Chen et al., 2012).

The quantitative structure-activity relationship (QSAR) has been widely used to interpret and predict the toxicity mechanism of compounds (Harju et al., 2009; Li et al., 2013). Previous studies showed that QSARs could characterize the structure features affecting the binding affinity of chemicals to sex hormone binding globulin (SHBG) (Liu et al., 2016, 2017), affecting the octanol-air partition coefficient (K_{OA}) of OPFRs (Wang et al., 2017b), and affecting the binding constants of OPFRs interacting with tumor suppressor genes (*p53*) (Li et al., 2015).

In this study, the damages of fifteen typical OPFRs (chlorinated phosphates, alkyl phosphates, aryl phosphates, and halogenated phosphates) to simulated biofilms were determined by the electrochemical impedance spectroscopy (EIS) (Kwon et al., 2006). The molecular structure descriptors that characterize the actions mechanisms were screened by stepwise regression. The six molecular descriptors (*MATS7e, DLS_05, Mor19m, Mor22v, Mor12v* and *MATS8m*) were screened to study the actions between OPFRs and mimetic biomembrane. A QSAR model was developed by the partial least squares (PLS) method to study the microscopic mechanisms between the OPFRs and membranes.

2. Materials and methods

2.1. Materials

For the fifteen typical OPFRs (Table S1), triphenyl phosphate (TPP), tetraphenyl resorcinol bis(diphenylphosphate) (RDP), tripropyl phosphate (TPrP), tri-p-tolyl phosphate (TPTP), triethyl phosphate (TEP), 2-ethylhexyl diphenyl phosphate (EHDPP), tri-m-cresyl phosphate (TCrP), tris(2-chloroethyl) phosphate (TCEP), phosphoric acid tris(2-chloro-1-methylethyl) ester (TCBP), 2-sec-butyl-4,6-dinitrophenol (DnBP), tributyl phosphate (TBP), tris(2-butoxyethyl) phosphate (TBEP), bisphenol-A bis(diphenyl phosphate) (BDP), tri-m-tolylphosphate (TMTP) were purchased from Dr. Ehrenstorfer (Germany). Decane was purchased from Shanghai Maclean Biochemical Technology Co., Ltd. (Beijing, China). Powdered 1,2-dipalmitoyl-sn-glycero-3-phosphocholine (DPPC) and 1,2-dipal-mitoyl-sn-glycero-3-phosphothioethanol (DPPTE) were purchased from Avanti, USA. The other chemicals were all analytical reagents and used as received. The experimental water was purified by a Milli-Q purification system (Barnstead, USA) to a specific resistance (more than 18 M cm).

2.2. Construction of supported bilayer lipid membranes (s-BLMs) on gold electrode

The gold electrode was polished primarily. The smoothed substrate was ultrasonically cleaned with ethanol then in ultrapure water to remove adhesive particles. The electrode was then placed in a solution and washed with pure water. The clean electrode was scanned by cyclic voltammetry (CV) to remove impurities on its surface. After scanning, the electrode was washed with ultrapure water and dried for use.

A clean bare gold was immersed in DPPTE solution, which made DPPTE molecule covalently bond to gold through forming "Au−S″ bond, thereby forming self-assembled monolayers (SAMs). Subsequently, the electrode was immersed in KCl solution to produce layers under hydrophilic/hydrophobic interaction. Thus, an s-BLMs modified gold electrode was prepared to serve as mimetic biomembrane.

2.3. Electrochemical measurements

The EIS method has been used to characterize the structural changes of mimetic biofilms (Chen et al., 2012; Harris and Bruening, 2000). In this study, the electrochemical measurements of s-BLMs

were performed on the three-electrode system by CHI 760D electrochemical analyzer. The impedance was supported and confirmed by EIS measurements. The experimental results of EIS were fitted by the equivalent circuit diagram (Fig. S1) obtained by Zview 3.1 software.

2.4. Data set

The logarithm of Y (log$Y$) was used as the dependent variable in the QSAR model. log$Y$ was defined as:

$$\log Y = \log\left(\frac{R_{m(1.5nM)}}{R_{m(DMSO)}}\right) \quad (1)$$

where $R_{m(1.5nM)}$ and $R_{m(DMSO)}$ were the impedance of s-BLMs of the tested OPFRs and DMSO. The molecular structures of fifteen typical OPFRs were drawn by ChemDraw Ultra, and initially optimized with minimum energy method (at the minimum RMS gradient of 0.001) to obtain the lowest energy structures in the Chem3D Ultra. The 4885 molecular descriptors were calculated by the DRAGON software (version 6.0) (Talete, 2012). These descriptors covered atom type and mass, topology and geometric parameters, three-dimensional arrangement and structure, drug-like index, etc. The screened molecular descriptors were used as the independent variables in the QSAR model.

2.5. Development of QSAR model

The fourteen descriptors (*MATS7e, DLS_05, Mor19m, Mor22v, Mor31p, Mor12v, MATS5p, R6u+, H7u, GATS7v, MATS8m, R4e+, G2m* and *SpMAD_B(m)*) were screened by stepwise regression analysis from the initial 4885 molecular descriptors. The values of fourteen molecular descriptors were listed in Table S2. Partial least squares (*PLS*) algorithm was performed for the model development. The number of significant *PLS* components (A) was determined by variable importance of projection (*VIP*) scores and the variance ratio of dependent variable (Q^2_{CUM}). The optimal model was selected with the largest Q^2_{CUM}.

The statistical parameters R^2_{adj} (adjusted multiple coefficient of determination), F and SE (Standard Error) (eqs (2)–(5)) to assess the significance of the model and goodness of fit (Qin et al., 2009).

$$R^2 = \sum_{i=1}^{n}(\hat{y}_i - \bar{y})^2 \Big/ \sum_{i=1}^{n}(y_i - \bar{y})^2 \quad (2)$$

$$R^2_{adj} = 1 - \left(1 - R^2\right)\frac{n-1}{n-p-1} \quad (3)$$

$$F = \left(1 + \frac{n-1-p}{p}R_{adj}{}^2\right)\Big/\left(1 - R_{adj}{}^2\right) \quad (4)$$

$$SE = \sqrt{\sum_{i=1}^{n}(y_i - \hat{y}_i)/(n-1)} \quad (5)$$

where y_i represented the observed value of i, $\hat{y}_i$ represented the predicted value of i, n represented the number of sample, p represented the number of predictors.

The Q^2 (cross-validation coefficient) was calculated (eq (6)) to assess the robustness of the model. The robustness was characterized by internal verification (OECD, 2007). Following analysis, training subsets were constructed by part of the OPFRs randomly selected. The selected variables were fitted to the subset and obtained the equation and predict the remaining OPFRs. This procedure was repeated ten times. The average Q^2_{IN} (internal cross-validation coefficient) was taken. If Q^2_{IN} was slightly different from it in optimal model, the robustness of the model was better.

$$Q^2 = 1 - \frac{\sum_{i=1}^{n}\left(y_i - \hat{y}_{i/i}\right)^2}{\sum_{i=1}^{n}(y_i - \bar{y})^2} \quad (6)$$

where $\hat{y}_{i/i}$ represented the predicted value of model without i, $\bar{y}$ represented the mean of the observed value, m represented the number of observations in validation set.

The application domain (AD) of the QSAR model was accessed by the Euclidean distance-based approach and Williams plot (Li et al., 2012; Liu et al., 2016). The Euclidean distances were drawn by the ambit discovery v0.04 software (http://ambit.sourceforge.net/download_ambitdiscovery.html). The Williams plot of the standard residuals (δ) versus leverage values (h_i) illustrated that data set had no outliers with the standard residual of compounds within (−2.5, +2.5). δ expressed as eq (7).

$$\delta = (y_i - \hat{y}) \Big/ \sqrt{\sum_{i=1}^{n}(y_i - \hat{y}_i) \Big/ (n - A - 1)} \quad (7)$$

when $h_i < h^*$ (warning leverage value), there was no compound in data set that significantly influenced the regression of the model. h_i, h expressed as eqs (8) and (9) (Li et al., 2012).

$$h_i = x_i^T\left(X^TX\right)^{-1}x_i \quad (8)$$

$$h^* = 3(p+1)/n \quad (9)$$

where x_i was the descriptor vector of the i-th compound, X was the descriptor matrix, X^T, x_i^T was the transpose of x_i and X; A represented the number of significant *PLS* components.

3. Results and discussion

3.1. Characterization of simulated biofilm

The EIS was used to evaluate the integrity of s-BLMs on gold electrode surface. The resistances were well fitted by Zview 3.1 software because the relative error (Error%) of each component was less than 5%. The non-conductive of the s-BLMs blocked electron transferred between the electrode interface and the electrolyte, so the integrity of s-BLM could be characterized by the impedance of the modified gold electrode. The impedance R_m reached $4.64 \times 10^6\,\Omega$ (Table 1) indicating the integrity of the s-BLMs constructed in this work.

3.2. Identifying test concentrations of OPFRs

The electrochemical behaviors of OPFRs with different concentrations were characterized by impedance of the s-BLM. One previous study showed that curcumin interacted with the simulated

Table 1
Fitting data and relative errors of each component.

component	$R_s(\Omega)$	$R_m(\Omega)$	Q_m-CPE-T	Q_m-CPE-P
Fitting data	71.32	4.64×10^6	4.98×10^{-7}	7.5×10^{-1}
Relative error(%)	4.36	1.58	2.80×10^{-1}	2.25

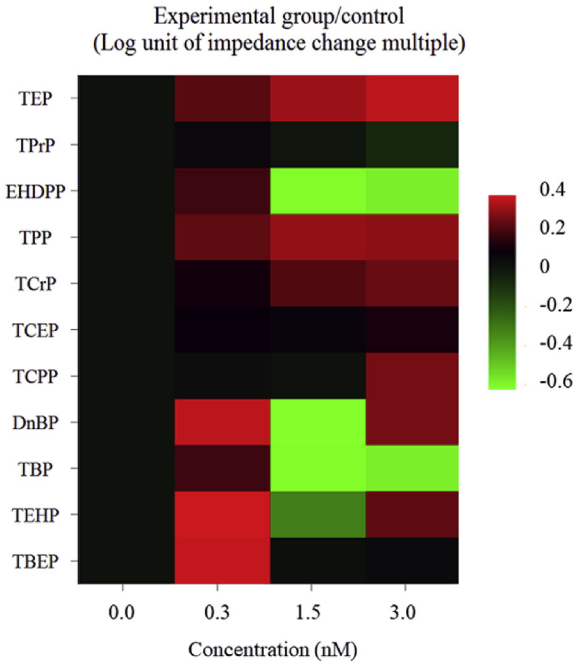

Fig. 1. Heatmap of impedance of typical OPFRs.

biofilms in a concentration-dependent manner (Chen et al., 2012). The low concentration of compound tended to insert into the outer layer of membrane causing steric hindrance increased. The increased hindrance blocked the electron transfer between the probe and the electrode which resulted in higher impedance values. The high concentration of compound caused the impedance reduction as the compound acted as a medium between the electrode and probe. In order to determine the optimal concentration of OPFRs on the membrane, impedance values of eleven OPFRs were measured with three concentration gradients (0.3 nM, 1.5 nM and 3.0 nM) (Table S3) (Gibson et al., 2019). Cluster analysis of different concentration was revealed by a heatmap. Heatmap showed the impedance variance across multiple concentrations of each type of OPFRs. According to the heatmap (Fig. 1), the impedances of typical OPFRs possessed good homogeneity under the concentration of 1.5 nM that was then used as the test concentration.

3.3. QSAR model for typical OPFRs

In this study, six molecular descriptors, including *MATS7e, DLS_05, Mor19m, Mor22v, Mor12v* and *MATS8m*, were screened as independent variables. Parameters of screened descriptors were listed in Table 2. The optimal model obtained by PLS analysis was:

$$\log Y = 1.50 \times MATS7e - 5.74 \times 10^{-1} DLS\_05 + 4.64 \times 10^{-1} Mor19m - 4.66 \times 10^{-1} Mor22v + 5.60 \times 10^{-2} Mor12v - 4.87 \times 10^{-2} MATS8m + 4.63 \times 10^{-1}$$

$$n = 15,\ R^2_{adj} = 0.962,\ A = 3,\ F = 26.32,\ R^2_Y = 0.970,\ Q^2_{CUM} = 0.913,\ Q^2_{IN} = 0.874,\ SE = 0.065,\ p < 0.001$$

The values of R^2_{adj}, R^2_Y, Q^2_{CUM} and Q^2_{IN} all showed the goodness-of-fit and robustness of model. The distance between R^2_Y and Q^2_{CUM} was 0.3, indicating that the model was not overmatched (OECD, 2007). The plots of observed log*Y* versus predicted log*Y* (Fig. 2) illustrated the good interpretability of model.

3.4. Applicability domain

The applicability domain (AD) was characterized by the Euclidean distance-based method and Williams plots (Fig. 3). The Euclidean distance for the model showed that all OPFRs located in the acceptable region (Fig. 3A), indicating that the training set of model was representative (Yang et al., 2016). Williams plots showed that the δ of the compound was less than 2.5, and the h_i was less than the warning value of 1.40. These confirmed that no chemicals could be identified as outliers (Fig. 3B). No outliers and miscalculations in AD ensured the credibility of the model.

Table 2
The observed and predicted log*Y* values of considered compounds and molecular descriptors in the developed QSAR model.

No.	Compounds	log*Y*			*MATS7e*[a]	*DLS_05*[b]	*Mor19m*[c]	*Mor22v*[d]	*Mor12v*[e]	*MATS8m*[f]
		Observed	Predicted	Residuals						
1	TEP	2.85×10^{-1}	2.53×10^{-1}	3.19×10^{-2}	0.203	1.00	0.055	−0.194	−0.487	0.589
2	TPrP	-1.05×10^{-2}	2.73×10^{-2}	-3.78×10^{-2}	0.078	1.00	0.172	0.015	−0.810	0.136
3	EHDPP	-6.26×10^{-1}	-5.04×10^{-1}	-1.22×10^{-1}	−0.263	1.00	0.096	0.060	−0.453	−0.167
4	TPP	2.79×10^{-1}	3.46×10^{-1}	-6.69×10^{-2}	−0.176	0.00	0.192	−0.06	0.421	−0.101
5	TCrP	1.89×10^{-1}	2.72×10^{-1}	-8.25×10^{-2}	−0.171	0.50	0.559	−0.134	0.280	−0.274
6	TCEP	4.32×10^{-2}	4.47×10^{-2}	-1.59×10^{-3}	0.005	1.00	0.347	−0.047	−0.617	0.017
7	TCPP	8.72×10^{-2}	1.15×10^{-1}	-2.74×10^{-2}	0.078	1.00	0.425	0.083	−0.848	0.060
8	DnBP	-6.43×10^{-1}	-6.43×10^{-1}	-1.11×10^{-4}	−0.753	0.50	0.579	−0.017	−0.226	−0.875
9	TBP	-6.26×10^{-1}	-6.06×10^{-1}	-2.07×10^{-2}	−0.346	1.00	0.307	0.133	−1.113	−0.081
10	TEHP	-3.27×10^{-1}	-3.88×10^{-1}	6.06×10^{-2}	−0.340	1.00	1.338	0.598	−2.083	−0.112
11	TBEP	3.57×10^{-3}	-1.08×10^{-1}	1.12×10^{-1}	−0.228	1.00	0.667	−0.203	−1.242	−0.176
12	BDP	1.60×10^{-1}	8.13×10^{-2}	7.84×10^{-2}	−0.191	0.00	−0.154	0.067	−0.048	−0.182
13	RDP	4.52×10^{-2}	-3.30×10^{-2}	7.82×10^{-2}	−0.230	0.00	−0.69	−0.199	1.377	0.045
14	TMTP	-4.06×10^{-1}	-4.06×10^{-1}	3.10×10^{-4}	−0.624	0.50	0.505	−0.182	0.479	−0.106
15	TPTP	5.77×10^{-1}	5.78×10^{-1}	-1.46×10^{-3}	0.048	0.50	0.434	−0.205	0.297	−0.335

[a] *MATS7e* is 2D autocorrelations of lag 7/weighted by atomic Sanderson electronegativities.
[b] *DLS_05* is modified drug-like score.
[c] *Mor19m* is 3D-MoRSE descriptors of signal 19/weighted by atomic masses.
[d] *Mor22v* is 3D-MoRSE - signal 22/weighted by atomic van der Waals volumes.
[e] *Mor12v* is 3D-MoRSE - signal 12/weighted by atomic van der Waals volumes.
[f] *MATS8m* is 2D autocorrelations of lag 8/weighted by atomic masses.

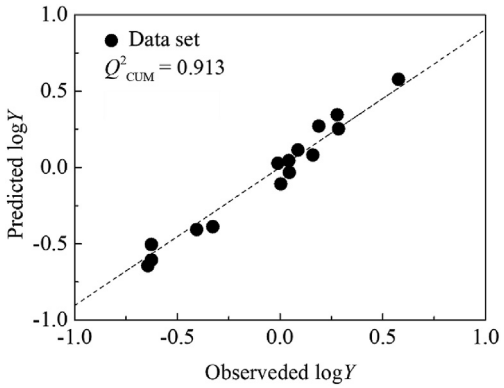

Fig. 2. The fitted plot of measured and predicted values of log*Y*.

4. Mechanism interpretation

The QSAR model extracted six molecular descriptors (*MATS7e*, *DLS_05*, *Mor19m*, *Mor22v*, *Mor12v* and *MATS8m*). *MATS7e* and *MATS8m* were 2D autocorrelations weighted by atomic Sanderson electronegativities and atomic masses. The 2D-autocorrelation descriptors were generally used to describe the distribution of atomic properties along the topological structures (Sliwoski et al., 2016). The variable *MATS7e* denoted the interactions between each pair of atoms at the topological distance equal to 7, while *MATS8m* accounted for the interaction of pair atoms at the topological distance equal to 8 (Liu et al., 2015). *DLS_05* represented the modified drug-like-score, which accounted for a set of properties, including the number of H-bond donors, H-bond acceptors, lipophilicity and unsaturation index (Rasulev et al., 2017). *DLS* descriptor had been used to develop a model showing that chemicals with low drug-like-score values were not suitable for the actions with biological systems (Rasulev et al., 2017). *Mor19m*, *Mor22v* and *Mor12v*, among the 3D-MoRSE descriptors, were part of geometrical descriptors. *Mor19m* was weighted by atomic masses, while *Mor22v* and *Mor12v* weighted with atomic van der Waals volumes, respectively. The 3D-MoRSE descriptors were based on the idea of transforming the information of 3D atomic coordinates used to prepare theoretical scattering curves in electron diffraction research (Duchowicz et al., 2006). The values of these descriptors could represent specific information in a certain three-dimensional structure space. The *Mor22v* and *Mor12v* descriptors, calculated by different angular scattering functions, showed the three-dimensional arrangement of the atoms modifying the size and shape of molecule (Asadollahi-Baboli, 2016; Devinyak et al., 2014). The large spatial structures and space arrangements of the compounds made it difficult to pass through the biofilm.

Table 3
VIP values and PLS weights for the QSAR model.

Variables	*VIP*	$W^*_C[1]$	$W^*_C[2]$	$W^*_C[3]$
MATS7e	1.47	0.702	0.811	0.555
Mor19m	1.04	−0.296	−0.237	−0.911
DLS_05	0.879	−0.218	0.657	0.783
MATS8m	0.855	−0.402	0.021	−0.156
Mor22v	0.802	0.308	−0.181	0.187
Mor12v	0.782	0.339	−0.022	−0.568

Table 3 listed the variable importance of projection (*VIP*) and PLS weights for the optimal model. The distribution of atomic electronegativities (*MATS7e*) was the primary factor influencing the actions between OPFRs and simulated biofilms (Fig. 4). Various substituents caused different values of molecular structure descriptors in the QSAR model. The *MATS7e* had relation to the electrophilicity of substituted group. The halogen atoms, oxygen atoms, nitrogen atoms and aromatic rings in the substituent made the significant difference in electronegativity. The significant difference made chemicals strongly attract the electrons. Accumulation of negative charges on the inner side of the membrane caused the chemical could invade the inside of the biofilm thus destroying the membrane structure (Ma et al., 2017). This was consistent with the electrochemical detection. The compounds with electronegative atoms could invade the inner layer of membrane and destroy its integrity which resulted in low impedance values. The relative values of molecular structure descriptors of DnBP (*MATS7e* = −0.753, *Mor19m* = 0.579) and TCrP (*MATS7e* = −0.171, *Mor19m* = 0.559) were listed in Table 2. The values of *Mor19m* for both two chemicals were similar. The nitro substituent groups on DnBP had higher electron affinity than aromatic group on TCrP. That difference in electronegativity implied that DnBP could easily cause changes in cell membrane and damage its integrity compared to TCrP. It agreed with the electrochemical experiments. The impedance of DnBP was significantly lower than that of TCrP (−0.643 and 0.189, respectively). Kong et al. found that DnBP could affect membrane receptor integrin *αvβ3* and ERK1/2 signaling pathway to disrupt the thyroid system (Kong et al., 2018). TCEP containing a chlorine atom could cause changes in cell membrane

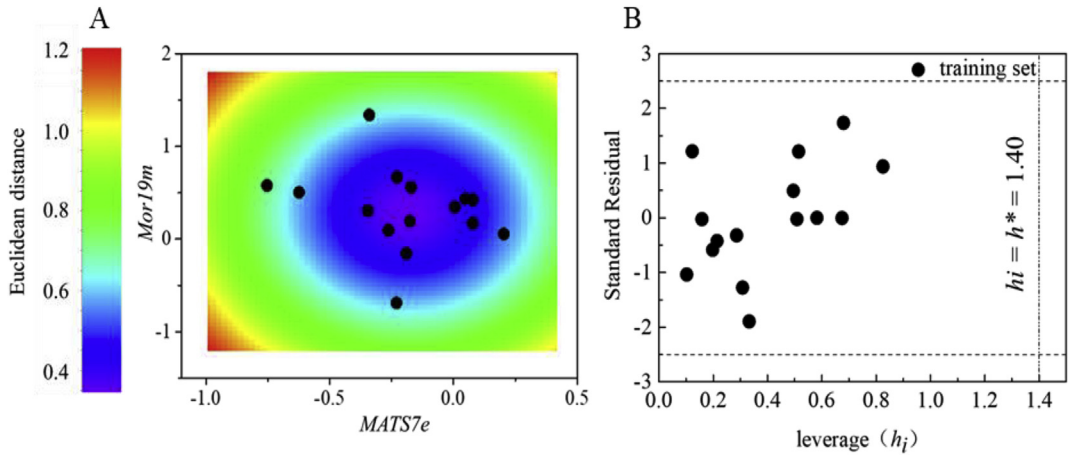

Fig. 3. Applicability domains for the QSAR model. (A) AD characterized by the Euclidean distance-based approach. (B) Plot of standardized residuals versus leverages (h_i). The transverse dash lines represent ±2.5 standardized residual, the vertical dotted line represents warning leverage ($h^* = 1.40$).

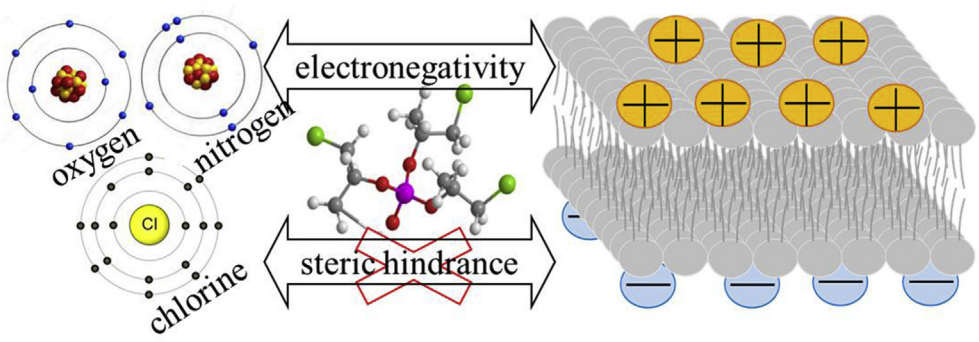

Fig. 4. Primary factor for the actions between OPFRs and mimetic biomembrane.

composition and membrane function integrity (Yang et al., 2018). And TCEP also could interfere the $p21^{Waf1/Cip1}$-Rb pathway to induce senescence in the human L02 hepatocytes (Zhang et al., 2017).

Moreover, the distribution of atomic mass (*Mor19m*) was another important factor affecting the actions. This descriptor was positively correlated with the steric hindrance. The compounds with significant spatial structures of particle could be difficult to invade the inner layer of membrane (Fig. 4). The impedance rose with the increase of steric hindrance. As shown in Table 2, EHDPP and TCrP were both substituted by aromatic rings. The value of *MATS7e* for EHDPP and TCrP were −0.263 and −0.171 respectively, suggesting that the electron-withdrawing property of substituent had slight difference. The *Mor19m* of EHDPP and TCrP were 0.096 and 0.559 separately, showing that TCrP had larger steric hindrance than EHDPP. The impedance of TCrP (0.189) was higher than that of EHDPP (−0.626) resulted from the steric effect. The steric effects alleviated the impairment to membrane integrity caused by the electronegativities of compounds.

5. Conclusion

In this study, the QSAR model was developed to study the damage of fifteen typical OPFRs (chlorinated phosphates, alkyl phosphates, aryl phosphates, and halogenated phosphates) to simulated biofilms. Statistical results indicated the QSAR model could be a useful tool for mechanism interpretability within the application domain. The results indicated that the impedance of simulated biofilms was governed by their electronegativities (*MATS7e*) and spatial structures (*Mor19m*). Electron-withdrawing substituents had a marked destructing effect on the integrity of biomembrane while the steric hindrance alleviated the impairment. Moreover, other characters (the drug-like index, spatial structures of particle and distribution of atomic masses) also contributed to the actions.

Acknowledgments

This research was supported by the National Natural Science Foundation of China (41530642, 21677173) and the Youth Innovation Promotion Association CAS (2017255, 2015169).

Appendix A. Supplementary data

Supplementary data to this article can be found online at https://doi.org/10.1016/j.chemosphere.2019.03.130.

References

Asadollahi-Baboli, M., 2016. *In silico* evaluation, molecular docking and QSAR analysis of quinazoline-based EGFR-T790M inhibitors. Mol. Divers. 20, 729–739.
Chen, G., Chen, Y., Yang, N., Zhu, X., Sun, L., Li, G., 2012. Interaction between curcumin and mimetic biomembrane. Sci. China Life Sci. 55, 527–532.
Chen, G., Jin, Y., Wu, Y., Liu, L., Fu, Z., 2015. Exposure of male mice to two kinds of organophosphate flame retardants (OPFRs) induced oxidative stress and endocrine disruption. Environ. Toxicol. Pharmacol. 40, 310–318.
Devinyak, O., Havrylyuk, D., Lesyk, R., 2014. 3D-MoRSE descriptors explained. J. Mol. Graph. Model. 54, 194–203.
Dishaw, L.V., Powers, C.M., Ryde, I.T., Roberts, S.C., Seidler, F.J., Slotkin, T.A., Stapleton, H.M., 2011. Is the pentaBDE replacement, tris (1,3-dichloro-2-propyl) phosphate (TDCPP), a developmental neurotoxicant? Studies in PC12 cells. Toxicol. Appl. Pharmacol. 256, 281–289.
Duchowicz, P.R., Fernández, M., Caballero, J., Castro, E.A., Fernández, F.M., 2006. QSAR for non-nucleoside inhibitors of HIV-1 reverse transcriptase. Bioorg. Med. Chem. 14, 5876–5889.
Gibson, E.A., Stapleton, H.M., Calero, L., Holmes, D., Burke, K., Martinez, R., Cortes, B., Nematollahi, A., Evans, D., Anderson, K.A., Herbstman, J.B., 2019. Differential exposure to organophosphate flame retardants in mother-child pairs. Chemosphere 219, 567–573.
Gu, Y., Yang, Y., Wan, B., Li, M., Guo, L.H., 2018. Inhibition of O-linked N-acetylglucosamine transferase activity in PC12 cells - a molecular mechanism of organophosphate flame retardants developmental neurotoxicity. Biochem. Pharmacol. 152, 21–33.
Harju, M., Hamers, T., Kamstra, J.H., Sonneveld, E., Boon, J.P., Tysklind, M., Andersson, P.L., 2009. Quantitative structure-activity relationship modeling on *in vitro* endocrine effects and metabolic stability involving 26 selected brominated flame retardants. Environ. Toxicol. Chem. 26, 816–826.
Harris, J.J., Bruening, M.L., 2000. Electrochemical and in situ ellipsometric investigation of the permeability and stability of layered polyelectrolyte films. Langmuir 16, 2006–2013.
Kim, J.-W., Isobe, T., Sudaryanto, A., Malarvannan, G., Chang, K.-H., Muto, M., Prudente, M., Tanabe, S., 2013. Organophosphorus flame retardants in house dust from the Philippines: occurrence and assessment of human exposure. Environ. Sci. Pollut. Res. 20, 812–822.
Kong, D., Liu, Y., Zuo, R., Li, J., 2018. DnBP-induced thyroid disrupting activities in GH3 cells via integrin $\alpha v\beta 3$ and ERK1/2 activation. Chemosphere 212, 1058–1066.
Kwon, N.-H., Rahman, M.A., Won, M.-S., Shim, a.Y.-B., 2006. Lipid-bonded conducting polymer layers for a model biomembrane. Anal. Chem. 78, 52–56.
Li, F., Cao, L., Li, X., Li, N., Wang, Z., Wu, H., 2015. Affinities of organophosphate flame retardants to tumor suppressor gene p53: an integrated *in vitro* and *in silico* study. Toxicol. Lett. 232, 533–541.
Li, F., Wu, H., Li, L., Li, X., Zhao, J., Peijnenburg, W.J., 2012. Docking and QSAR study on the binding interactions between polycyclic aromatic hydrocarbons and estrogen receptor. Ecotoxicol. Environ. Saf. 80, 273–279.
Li, X., Wang, X., Shi, W., Liu, H., Yu, H., 2013. Analysis of Ah receptor binding affinities of polybrominated diphenyl ethers via *in silico* molecular docking and 3D-QSAR. SAR QSAR Environ. Res. 24, 75–87.
Liu, H., Yang, X., Lu, R., 2016. Development of classification model and QSAR model for predicting binding affinity of endocrine disrupting chemicals to human sex hormone-binding globulin. Chemosphere 156, 1–7.
Liu, H., Yang, X., Yin, C., Wei, M., He, X., 2017. Development of predictive models for predicting binding affinity of endocrine disrupting chemicals to fish sex hormone-binding globulin. Ecotoxicol. Environ. Saf. 136, 46–54.
Liu, Y., Winkler, D.A., Epa, V.C., Zhang, B., Yan, B., 2015. Probing enzyme-nanoparticle interactions using combinatorial gold nanoparticle libraries. Nano Res. 8, 1293–1308.
Ma, Y., Poole, K., Goyette, J., Gaus, K., 2017. Introducing membrane charge and membrane potential to T cell signaling. Front. Immunol. 8, 1–11.

Marklund, A., Andersson, B., Haglund, P., 2003. Screening of organophosphorus compounds and their distribution in various indoor environments. Chemosphere 53, 1137–1146.
Moller, A., Sturm, R., Xie, Z., Cai, M., He, J., Ebinghaus, R., 2012. Organophosphorus flame retardants and plasticizers in airborne particles over the Northern Pacific and Indian Ocean toward the Polar Regions: evidence for global occurrence. Environ. Sci. Technol. 46, 3127–3134.
OECD, 2007. Guidance Document on the Validation of (Quantitative) Structure-Activity Relationships [QSAR] Models. Available online at: http://www.oecd.org/dataoecd/55/22/38131728.pdf.
Qin, H., Chen, J., Wang, Y., Wang, B., Li, X., Li, F., Wang, Y., 2009. Development and assessment of quantitative structure-activity relationship models for bioconcentration factors of organic pollutants. Chin. Sci. Bull. 54, 628–634.
Rasulev, B., Jabeen, F., Stafslien, S., Chisholm, B.J., Bahr, J., Ossowski, M., Boudjouk, P., 2017. Polymer coating materials and their fouling release activity: a cheminformatics approach to predict properties. ACS Appl. Mater. Interfaces 9, 1781–1792.
Reemtsma, T., Quintana, J.B., Rodil, R., García-López, M., Rodrıguez, I., 2008. Organophosphorus flame retardants and plasticizers in water and air I. Occurrence and fate. Trac. Trends Anal. Chem. 27, 727–737.
Ren, G., Hu, J., Shang, Y., Zhong, Y., Yu, Z., An, J., 2017. Tributylphosphate (TBP) and tris (2-butoxyethyl) phosphate (TBEP) induced apoptosis and cell cycle arrest in HepG2 cells. Toxicol. Res.,UK 6, 902–911.
Ren, X., Lee, Y.J., Han, H.J., Kim, I.S., 2008. Effect of tris-(2-chloroethyl)-phosphate (TCEP) at environmental concentration on the levels of cell cycle regulatory protein expression in primary cultured rabbit renal proximal tubule cells. Chemosphere 74, 84–88.
Sliwoski, G., Mendenhall, J., Meiler, J., 2016. Autocorrelation descriptor improvements for QSAR: 2DA_Sign and 3DA_Sign. J. Comput. Aided Mol. Des. 30, 209–217.
Talete, srl, 2012. Dragon (Software for Molecular Descriptor Calculation) Version 6.0. http://www.Talete.Mi.It/.
Van den Eede, N., Dirtu, A.C., Neels, H., Covaci, A., 2011. Analytical developments and preliminary assessment of human exposure to organophosphate flame retardants from indoor dust. Environ. Int. 37, 454–461.
van der Veen, I., de Boer, J., 2012. Phosphorus flame retardants: properties, production, environmental occurrence, toxicity and analysis. Chemosphere 88, 1119–1153.
Wang, G., Shi, H., Du, Z., Chen, H., Peng, J., Gao, S., 2017a. Bioaccumulation mechanism of organophosphate esters in adult zebrafish (*Danio rerio*). Environ. Pollut. 229, 177–187.
Wang, Q., Zhao, H., Wang, Y., Xie, Q., Chen, J., Quan, X., 2017b. Determination and prediction of octanol-air partition coefficients for organophosphate flame retardants. Ecotoxicol. Environ. Saf. 145, 283–288.
Wang, S., Wan, B., Zhang, L., Yang, Y., Guo, L.H., 2014. *In vitro* inhibition of lysine decarboxylase activity by organophosphate esters. Biochem. Pharmacol. 92, 506–516.
Wu, L., Jiang, X., 2016. Recent developments in methodology employed to study the interactions between nanomaterials and model lipid membranes. Anal. Bioanal. Chem. 408, 2743–2758.
Yang, W., Zhao, F., Fang, Y., Li, L., Li, C., Ta, N., 2018. ^{1}H-nuclear magnetic resonance metabolomics revealing the intrinsic relationships between neurochemical alterations and neurobehavioral and neuropathological abnormalities in rats exposed to tris(2-chloroethyl)phosphate. Chemosphere 200, 649–659.
Yang, X., Liu, H., Yang, Q., Liu, J., Chen, J., Shi, L., 2016. Predicting anti-androgenic activity of bisphenols using molecular docking and quantitative structure-activity relationships. Chemosphere 163, 373–381.
Zhang, Q., Lu, M., Dong, X., Wang, C., Zhang, C., Liu, W., Zhao, M., 2014. Potential estrogenic effects of phosphorus-containing flame retardants. Environ. Sci. Technol. 48, 6995–7001.
Zhang, W., Zhang, Y., Hou, J., Xu, T., Yin, W., Xiong, W., Lu, W., Zheng, H., Chen, J., Yuan, J., 2017. Tris (2-chloroethyl) phosphate induces senescence-like phenotype of hepatocytes via the p21$^{Waf1/Cip1}$-Rb pathway in a p53-independent manner. Environ. Toxicol. Pharmacol. 56, 68–75.